

Article

Provenance Analysis of the Ojén Nappe and Its Implication for the Geodynamic History (Alpujárride Complex, Betic Cordilleras, Spain)

José Julián Esteban *, Julia Cuevas and José María Tubía

Department of Geology, Faculty of Science and Technology, University of the Basque Country (UPV/EHU), Apto. 644, 48080 Bilbao, Spain

* Correspondence: jj.esteban@ehu.eus; Tel.: +34-946-01-24-53

Abstract: The Ojén nappe, an allochthonous unit that underlies the Ronda peridotites (Betic Cordilleras), is composed of Triassic marbles overlying a metapelitic sequence. In order to carry out an LA-ICP-MS U-Pb age determination and provenance analysis, detrital zircon grains from two quartzites interlayered within marbles and metapelites were extracted. The obtained results yield the youngest zircon population of 254 ± 3 Ma (Late Permian) with a mean Th/U ratio of 0.34 that supports both the Permian–Triassic age of the marble member and the felsic magma nature for zircon-bearing protoliths. The Permian zircons exhibit tight age peaks in three main populations of 292 ± 2 Ma, 278 ± 3 Ma, and 254 ± 3 Ma, in agreement with the main age populations reported from rhyolites and shallow crustal basaltic–andesite subalkaline rocks emplaced in transtensional Permian basins of the Variscan Orogen during the break-up of Pangea. Moreover, the analyzed detrital zircon grains yield age distributions with clear Tonian–Stenian (ca. 950–975 Ma), Ediacaran–Cryogenian (ca. 560–615 Ma), Ordovician (ca. 460–465 Ma), and Cisuralian peaks (ca. 280–290 Ma) and smoothed Mesoproterozoic peaks that point to a weak and residual Cadomian peri-Gondwanan terrane inheritance. The identified Middle Ordovician detrital zircon populations (460–465 Ma) strengthen the hypothesis that the Alborán domain would be located along the southern passive margin of the European Hunic superterrane.

Keywords: peri-Gondwana; Betic Cordilleras; Ojén nappe; detrital zircon; LA-ICP-MS

Citation: Esteban, J.J.; Cuevas, J.; Tubía, J.M. Provenance Analysis of the Ojén Nappe and Its Implication for the Geodynamic History (Alpujárride Complex, Betic Cordilleras, Spain). *Minerals* **2023**, *13*, 569. <https://doi.org/10.3390/min13040569>

Received: 31 January 2023

Revised: 17 March 2023

Accepted: 13 April 2023

Published: 18 April 2023



Copyright: © 2023 by the authors. Licensee MDPI, Basel, Switzerland. This article is an open access article distributed under the terms and conditions of the Creative Commons Attribution (CC BY) license (<https://creativecommons.org/licenses/by/4.0/>).

1. Introduction

The Betic Cordilleras (south of Spain) and the Rif (north of Morocco) conform to the western termination of the peri-Mediterranean Alpine orogen. It is considered a collisional orogen disaggregated by an extensional collapse in a continuous convergence setting between the African and European plates from Cretaceous times onward [1]. The Betic Cordilleras consist of two main domains, referred to as the external and the internal zones that are located to the north and south of the belt, respectively. The external zone derives from Mesozoic and Cenozoic sediments formed on the southern paleomargin of the Variscan Iberian Massif. In contrast, the internal zone mainly encompasses metamorphic and highly deformed pre-Mesozoic rocks that are grouped in three allochthonous complexes, named in structural descending order: Maláguide, Alpujárride, and Nevado Filábride Complex.

The Ojén, Los Reales, and Guadaiza tectonic units compose the western part of the Alpujárride Complex [2] of the internal zones of the Betic Cordilleras. Until now, analyses on provenance and geodynamic evolution from detrital zircon studies were restricted to the Guadaiza nappe [3]. This work discusses the provenance and possible origin of detrital zircons populations in two samples of the Ojén nappe (tb-06-841 and tb-06-835), from zircon ages carried out using the LA-ICP-MS U-Pb method in combination with the determination of Th/U zircon ratios. The Ojén nappe crops out below the ultramafic massif of Sierra Alpujata (Figure 1). This massif, along with the Sierra Bermeja and Carratraca massifs,

conforms to the Ronda Peridotites, the largest worldwide exposure of the subcontinental lithospheric mantle, tectonically emplaced at Miocene times [4–8].

The Ojén nappe displays the typical lithological sequence described for the Alpujárride nappes, with Paleozoic or older metapelites at the bottom covered by a composite sequence, with quartzites at lower levels and a marble formation at the top [2]. A Triassic age is usually assumed for the Ojén marbles on the basis of their correlation with paleontologically dated marbles from the central and eastern nappes of the Alpujárride Complex [9–11]. Permo–Triassic ages are assigned to the underlying quartzites, whereas poorly constrained Paleozoic ages are attributed to the lowest metapelitic sequence (e.g., [12–14]). The available geochronological U–Pb SHRIMP data of the detrital zircon crystals from the carbonate series provide a maximum age of deposition of ca. 325 Ma [15]. However, recently published U–Pb LA-ICP-MS data from a detrital zircon population of a quartzite interlayered with marbles of the Guadaiza nappe [3] constraint the maximum depositional age at Early Permian times (ca. 289 Ma).

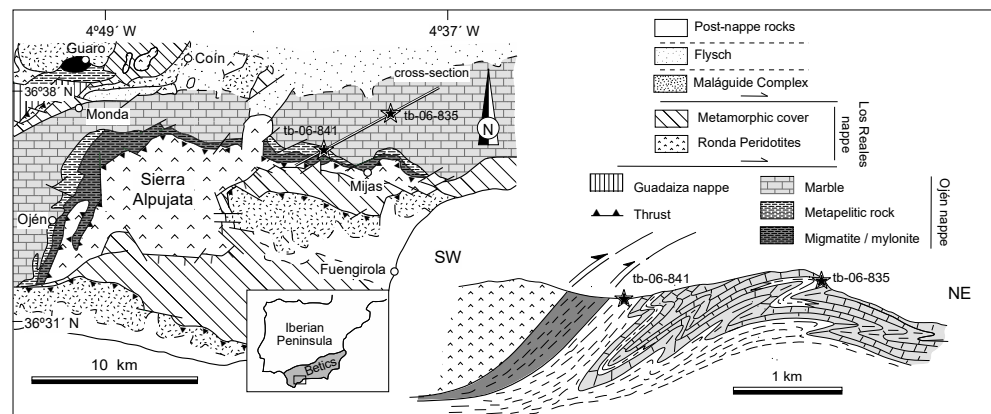


Figure 1. Geological map and cross-section of the Ojén nappe (taken from [16]) with studied sample (tb-06-841 and tb-06-835) locations (stars).

2. Sample Location

The studied quartzites from the Ojén nappe (Figure 1) come from different stratigraphic levels. The sample tb-06-835 belongs to a 10 m thick quartzite interlayered within the marble sequence (Figure 2A), whereas the sample tb-06-841 is a 1–1.5 m thick quartzite interlayered with metapelites in the transition zone between the metapelitic and marble sequences (Figure 2B).

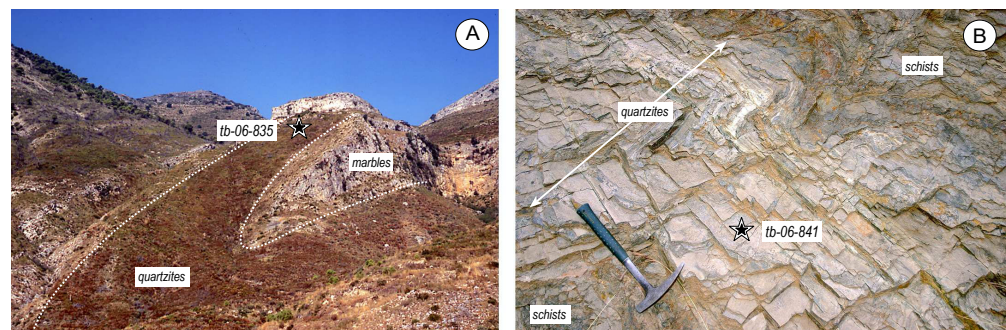


Figure 2. Outcrop views and locations of tb-06-835 (A) and tb-06-841 (B) quartzites.

Both samples were collected far enough away from the peridotite contact (see the cross-section in Figure 1) in order to minimize the local heating effect promoted by the high-temperature emplacement of the Ronda peridotites. The hot emplacement of the Ronda peridotites (e.g., Sierra Alpujata Massif) over the Ojén nappe during the Alpine Orogeny

produced a concordant dynamothermal aureole [17], with a maximum thickness of 700 m. This dynamothermal aureole is exposed over tens of kilometers along the northern border of the Sierra Alpujata Massif [17], where the marbles of the Ojén nappe crop out along the reverse limb (cross-section in Figure 1) of a large Alpine synform [18]. The dynamothermal aureole is composed of banded cordierite-bearing migmatites and leucocratic gneisses and contains interlayered retrogressed eclogites [19] and minor quantities of marbles. It was developed at high-temperature conditions at the expense of the metapelitic sequence. However, it is worth noting that a few zircon grains from both samples display very thin and dark luminescent external rims that yield Th/U values < 0.01 [16] and $^{206}\text{Pb}/^{238}\text{U}$ SHRIMP ages of ca. 20 to 22 Ma, which support the imprint of the thermal Miocene metamorphism [7,15,20].

3. Analytical Methods

Zircon grains from both quartzites were separated using conventional mineral separation techniques (crushing, sieving under 125 μm , Wilfley table, heavy liquids, and magnetic separation) in the Department of Geology of the University of the Basque Country. The extracted zircons were handpicked aleatory, mounted in epoxy resin (Struers Epofix, Madrid, Spain), and finally polished. Due to the different number of recovered zircons per sample, more zircons were mounted in tb-06-841 (193) than in tb-06-835 (163). In both cases, the number of grains per sample was higher than 117, the critical number suggested to achieve robust data of material provenance [21]. The internal structure of the zircon grains was recognized in backscattered electron (BSE) images (Supplementary Materials Figure S1), obtained using a scanning electron microscope (JEOL7000F-JSM, JEOL Ltd., Tokyo, Japan; operative conditions 20 kV, 8 nA and WD 10 mm). The zircons were analyzed using LA-ICP-MS at the University of the Basque Country (SGIker—Geochronology and Isotope Geochemistry Facility) using a 193 nm Resolution SE laser, with a pulse energy density of $\sim 6 \text{ J cm}^{-2}$ and a frequency of 5 Hz, coupled to a Thermo Fisher iCAP Qc quadrupole ICP-MS (Thermo Fisher Scientific, Waltham, MA, USA). The analytical spot size was 25 μm . The laboratory staff reduced the data using the Iolite 3.6 software package [22,23] and VizualAge [24] and provided the analytical tables. The data reduction process was carried out using the GJ-1 zircon standard for calibration [25] and Plesovice [26], 91500 [27], and BB40 zircon [28] as secondary standards. Ages in the text and figures are quoted always with concordance between 90% and 110% and as $^{206}\text{Pb}/^{238}\text{U}$ ages. The Tera–Wasserburg diagrams and weighted mean ages were produced using Isoplot/Ex 3.0 [29]. The distribution of zircon ages and the kernel density estimation (KDE) plots, with bin widths of 60 and 30, respectively, were calculated using DensityPlotter 8.5 [30].

4. LA-ICP-MS Results

4.1. Sample tb-06-841

One hundred and ninety-three detrital zircon grains were analyzed using LA-ICP-MS, only one hundred and seventy-seven of which, with concordance values ranging between 90% and 110%, were considered (Supplementary Materials Table S1). The measured Th/U ratios are between 0.03 and 1.98 (Figure 3). Most zircon grains ($n = 165$) have Th/U ratios greater than 0.1, and only twelve zircons display Th/U ratios < 0.1 . The age distribution patterns of the analyzed zircons are scattered between 219 Ma and 2986 Ma (Figure 4A). About 77% of them are from Precambrian ages that mostly group around Neoproterozoic (43%; ca. 542–994 Ma), Paleoproterozoic (15%; ca. 1666–2451 Ma), and minor Mesoproterozoic (6%; ca. 1013–1508 Ma) and Archean (3%; ca. 2503–2976 Ma) peaks. The remaining 23% of the analyzed ages are distributed in a mean Paleozoic (32%; ca. 255–538 Ma) and in minor Mesozoic (1%; ca. 219–244 Ma) peaks. Four main age populations at ~ 290 , ~ 465 , ~ 615 , and ~ 975 Ma can be recognized in KDE plots (Figure 4A). The youngest analyzed zircon has a Late-Triassic $^{206}\text{Pb}/^{238}\text{U}$ (219 Ma; Supplementary Materials Table S1) age, whereas a weighted mean age of 278 Ma (Figure 5A) is obtained from three zircon grains for the youngest zircon population (Early Permian–Cisuralian). A

last Permian zircon population of 293 Ma from six zircons was also calculated (Figure 5B). Both zircon populations display Th/U ratios > 0.21 (0.21–0.56; Supplementary Materials Table S1).

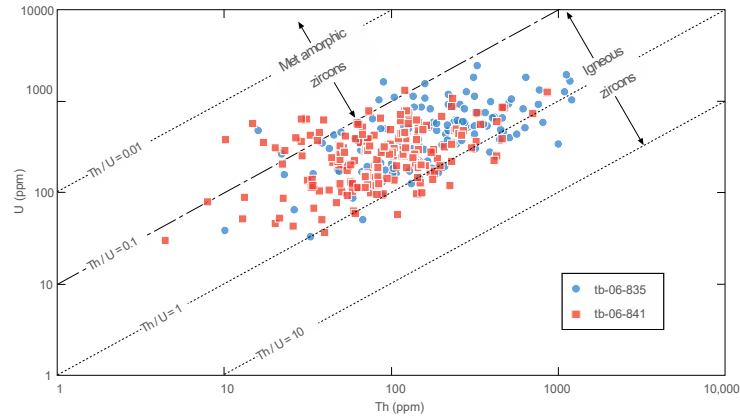


Figure 3. Th/U vs. $^{206}\text{Pb}/^{238}\text{U}$ age (Ma) of analyzed zircons of Ojén nappe’s quartzites.

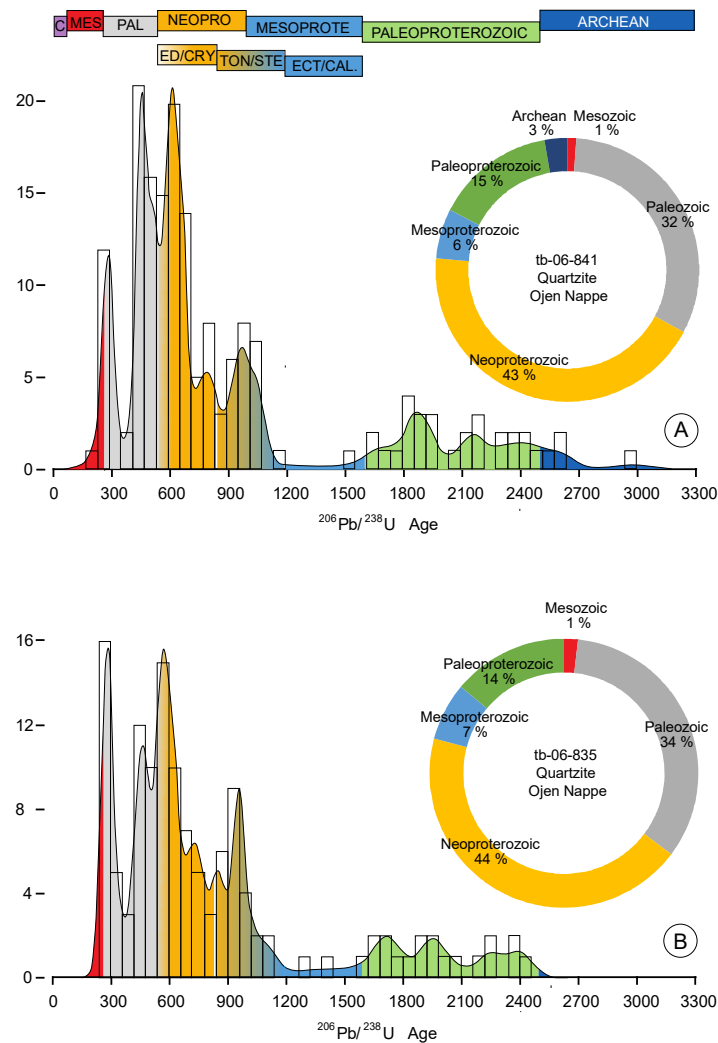


Figure 4. Kernel density estimation (KDE), histograms, and pie-chart age distribution plots of analyzed zircons of Ojén’s samples: (A) tb-06-841 and (B) tb-06-835.

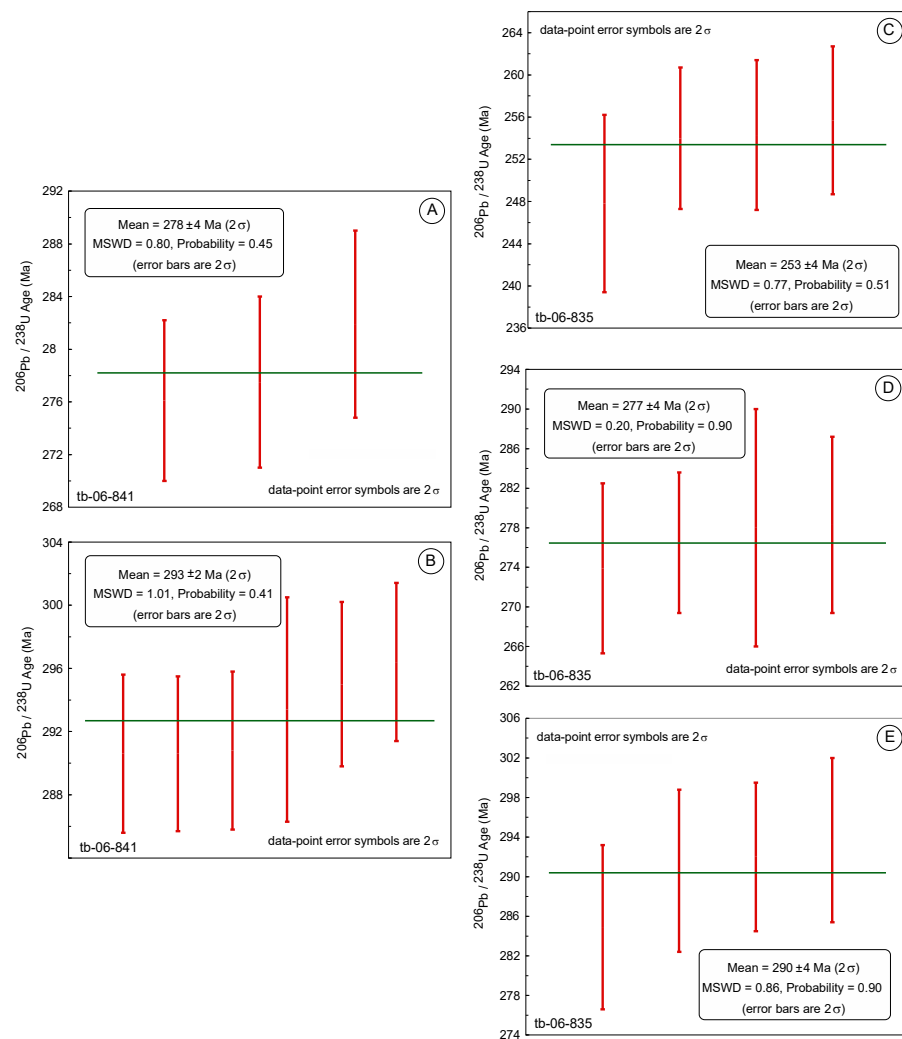


Figure 5. Weighted mean age of the youngest zircon populations: (A,B) from sample tb-06-841; (C–E) from sample tb-06-835.

4.2. Sample tb-06-835

One hundred and sixty-three detrital zircon grains were analyzed, and only one hundred and thirty have concordant ages between 240 Ma and 2430 Ma. The measured Th/U ratios ranged between 0.03 and 3.1. The overwhelming majority (126 out of 130) of these concordant zircon grains have Th/U > 0.1, a feature that supports the dominant magmatic origin of the zircon (Figure 3). The age distribution patterns (Figure 4B) show that 65% of the analyzed zircons are Precambrian in age, and mostly yield Neoproterozoic (44%; ca. 544–976 Ma) and Paleoproterozoic (14%; ca. 1651–2430 Ma) ages, with the rest being Mesoproterozoic (7%; ca. 1001–1561 Ma). The remaining analysis results reveal Paleozoic (34%; ca. 254–536 Ma) and Mesozoic (1%; ca. 240–248 Ma) ages. As in the previous sample, the same four main age populations exhibit peaks in the KDE plot at ~280, ~460, ~560, and 950 Ma (Figure 4B). The youngest measured zircon has a Middle Triassic $^{206}\text{Pb}/^{238}\text{U}$ (240 Ma; Supplementary Materials Table S1) age. Otherwise, a weighted mean of 253 Ma (Late Permian–Lopingian) for four zircons with high U contents (426–2299 ppm) and no metamictization textures (e.g., porous texture, patch zoning, cracks, and very dark BSE areas; Supplementary Materials Figure S1) characterize the youngest zircon population (Figure 5C). Two more Permian zircon populations of 277 Ma (from four zircons; Figure 5D) and 290 Ma (from four zircons; Figure 5E) were also found. All these three zircon populations display Th/U zircon ratios > 0.18 (0.18 to 1.07; Supplementary Materials Table S1).

5. Discussion

5.1. Deposition Age

The determination of the maximum depositional age of a sedimentary succession using radiometric methods (e.g., U-Pb zircon SHRIMP or LA-ICP-MS) can become a complex task, due to the possible resetting associated with superposed tectonothermal events. Therefore, the correct age determination of known pre- and post-sedimentation tectonothermal events is essential to avoid underestimation of the maximum depositional age of the sedimentary protolith of metamorphic rocks.

In this regard, the metamorphic record of the Ojén nappe is the result of (a) almost obliterated Late-Variscan metamorphism (e.g., [15,31]), and (b) the superposed Alpine metamorphism, associated with the short-lived and intense thermal metamorphism linked to the extensional collapse of the Betic Chain and the emplacement of Ronda peridotites [4–8]. In the two quartzite samples, the maximum depositional age must always be determined using the youngest inherited metamorphic or igneous zircon. In the tb-06-841 and tb-06-835 samples, the youngest pre-Alpine zircon grains display $^{206}\text{Pb}/^{238}\text{U}$ ages of 219 Ma (Late Triassic) and 240 Ma (Middle Triassic), respectively (Supplementary Materials Table S1). Both ages agree with the reported Triassic age for the Alpujarride marbles that have been paleontologically dated [12–14]. However, as the age resetting promoted by the superposed Alpine metamorphism (see Figure 6) could lead to Pb loss in some of the detrital zircon grains, the weighted mean age of the youngest zircon populations in each sample was considered a more conservative and appropriate estimation. By using this approach, an Early Permian–Cisuralian age of 278 ± 4 Ma is obtained from three zircons in tb-06-841 (Figure 5A), whereas an age of 253 ± 4 Ma (Late Permian–Early Triassic) is obtained from the four zircons of tb-06-835 (Figure 5C). Therefore, a maximum Permian age of 253 ± 4 Ma can be predicted for the sedimentation and the best radiometric estimation age of the carbonate sequence. Both zircon populations are younger than the age of the Late-Variscan metamorphism reported in the Betic Cordilleras [3,31], within others.

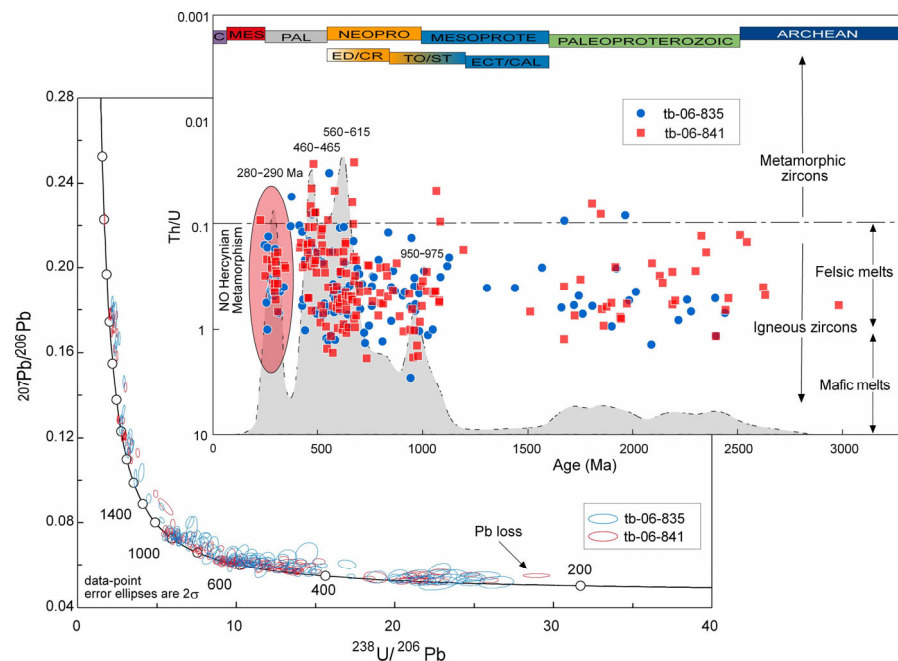


Figure 6. Tera–Wasserburg, KDE age distribution, and Th/U vs. age (Ma) distribution of analyzed samples. The KDE shows the integrated age distribution of both samples.

5.2. Zircon-Forming Events

The high proportion of Ediacaran–Cryogenian (44%–43%; 542–718 Ma), Paleozoic (34%–32%; 254–538 Ma), Tonian–Stenian (15%–14%; 718–1189 Ma), and Paleoproterozoic

(15%–14%; 1651–2451 Ma) ages observed in the KDE plots of both quartzites (Figure 6) define four main zircon populations: Cisuralian (280–290 Ma), Ordovician (460–465 Ma), Ediacaran–Cryogenian (560–615 Ma), and Tonian–Stenian (950–975 Ma). These populations contrasted with the scarcity of Mesoproterozoic (7%–6%; 1001–1561 Ma), Archean (3%; 2503–2976 Ma), and Mesozoic (1%; 219–248 Ma) zircon ages (Figure 6).

Zircon geochemistry can shed light on the origin of the zircon-bearing sedimentary protoliths. On this issue, the zircon Th/U ratio, although still subject to some uncertainty, is commonly used as a factor that allows igneous zircon ($\text{Th}/\text{U} > 0.1$) to be differentiated metamorphic ($\text{Th}/\text{U} < 0.1$) ones [32–34]. However, examples of metamorphic zircons crystallized at (ultra)high-temperature conditions with $\text{Th}/\text{U} > 0.1$ (e.g., [35–37]) and even igneous zircons with Th/U values lower than 0.1 have also been described [38,39]. Taking the two analyzed samples as a whole, 291 zircon grains yield Th/U ratios higher than 0.1, and only 16 grains have values below 0.1 (Figures 3 and 6). These data show that the dominant source for the above-referred zircon populations was igneous rocks. Moreover, the zircon Th/U ratio can also be used to study the composition of the melt in which zircon crystals grow, as Th/U ratios tend to be less than 1 in felsic melts and higher than 1 in mafic melts [33,40–42]. According to the mean Th/U ratio of 0.34 of the analyzed zircons, this additional constraint points to the magmatic rocks of felsic composition (Figure 6).

In the Betic Cordilleras, there are igneous rocks from magmatic events associated with different orogenic cycles that have to be tested as the first potential source materials. However, they can be easily excluded on the basis of two major criteria: the composition (felsic versus mafic) and the age of the magmatic events (253 ± 4 Ma). The external zone provides evidence of two magmatic events related to the Triassic–Jurassic extension that led to the opening of the westernmost branch of the Tethys Ocean: the older one is integrated by dolerite sheets and diabase dykes that intruded into the middle- and upper-Triassic rocks and the younger event as basaltic submarine flows with abundant pillow-lava structures within Jurassic sedimentary rocks [43,44]. It is clear that both its basic composition and its Mesozoic age prevent the consideration of the external zone as a provenance area. Similar reasons apply to invalidate most of the magmatic materials from the internal zones. For instance, the Nevado Filábride Complex contains an ultramafic unit, regionally referred to as Betic Ophiolitic Unit, that is characterized by numerous tectonic slices comprising eclogites and amphibolites derived from metamorphosed Jurassic gabbros [45,46]. These crustal rocks include abundant meta-granite and granitic orthogneisses (Lubrín gneisses), identified as syn-collisional granites, dated as Late Carboniferous [47]. Regarding the Alpujárride Complex, felsic magmatism of the Early Permian age has been recognized, represented by orthogneisses and migmatites linked to anatexis processes during a Variscan metamorphic event [3,31]. In the Torrox gneisses, Zeck and Whitehouse [31] described euhedral zircons showing rims with low Th/U values (average of 0.02), indicating an Early Permian age (285 ± 5 Ma). This value was interpreted as the age of the andalusite-bearing anatexis granite parent rock for the gneiss. In a recent work on the Istán migmatites of the Guadaiza nappe (western Alpujárride Complex), the prominent U-Pb LA-ICP-MS recorded peak at ca. 299 Ma for the Istán migmatites was considered the age of the Late-Variscan metamorphism that led to the anatexis and migmatization of the metapelitic sequence of this Alpujárride unit [3]. In the latter two cases, the mean Th/U ratio of the zircon grains was lower than 0.1, in contrast with the higher values (Th/U ratio > 0.1) recorded by most zircons from the two samples analyzed in this work (Figures 3 and 6). A second felsic magmatic process can be recognized within the Alpujárride Complex related to the hot emplacement of the Ronda peridotites, as it developed a dynamothermal aureole and partial melts that led to the intrusion of granite dykes in the peridotites during the Alpine Orogeny. An Early Miocene U-Pb SHRIMP age [8] has been attributed to the crystallization of granite dykes. Moreover, a Jurassic subvolcanic event comprising sheets of basic tholeiitic rocks interlayered within meta-evaporite is also recorded within the Triassic rocks of the Alpujárride Complex [43,48–50]. Finally, in the Maláguide Complex and the upper Alpujárride, there is a dyke system, but it can be excluded as a possible source because of its

Oligocene age and its doleritic composition [51–53]. In short, there are two characteristics of the Betic Cordilleras relevant to the provenance studies of their metasedimentary rocks: (1) the lack of large granite intrusions, and (2) that due to the age and geochemical inconsistencies described above, a source outside the Betic Cordilleras should be considered to be consistent with the age (Permian–Early Triassic) and the geochemical features' mean Th/U ratio of 0.34 of the zircon grains analyzed.

With the above considerations in mind, and taking into account the scarcity of Mesoproterozoic ages, the four zircon populations described in Section 5.1 (Figure 5) would point to (1) a zircon signature from the West African Craton instead of other cratons extensively affected by the Grenville Orogeny (Laurentia, Baltica, Avalonia, or Amazonia); (2) several provenance areas from the northern part of Gondwana such as the Pan-African Transhara belts, Metasaharan Craton, or the Tuareg shield; and (3) a peri-Gondwanan Cadomian terrane source related to the opening of the eastern branch of the Rheic Ocean at the Middle Ordovician time during the detachment of the Hunia supercontinent from Gondwana.

With the aim of constraining the most reliable source area, a more detailed zircon population distribution was analyzed from the youngest Permian zircons. In this case, as both samples had the same zircon populations, they were integrated together, resulting in three different Permian zircon populations (Figure 7A). These zircon populations display ages of 254 ± 3 Ma (Figure 7B; MSWD = 0.66; probability = 0.62; $n = 5$); 278 ± 3 Ma (Figure 7C; MSWD = 0.43; probability = 0.86; $n = 7$); and 292 ± 2 Ma (Figure 7D; MSWD = 0.96; probability = 0.47; $n = 10$), whereas measured Th/U ratios are in the ranges of 0.14–1.1, 0.23–0.53, and 0.18–0.56 (Supplementary Materials Table S1), respectively, for each zircon population. The recorded Permian ages (Cisuralian, Cissularian–Guadalupian, and Lopingian) correspond to the age clusters of rhyolites and shallow crustal, basaltic-andesite subalkaline rocks emplaced in transtensional Permian basins, linked to the crustal thinning, and the asthenospheric uplift due to the gravitational collapse of the Variscan Orogen during the break-up of Pangea (Iberian Massif, Pyrenees, Catalan Coastal Ranges, Iberian Range, French Central Massif, Sardinia, and Morocco [54]). The paleogeographical reconstruction of the westernmost Tethys realm for the Middle Triassic, performed on the basis of the different Triassic facies (Germanic vs. Alpine) and bioprovinces (Sephardician, Tethysian), place the Buntsandstein, Muschelkalk, and Keuper of the Germanic facies in the external and internal zone of the Betic Cordilleras [55]. However, the presence of Tethysian fauna, linked to the Alpine Triassic facies, is also confirmed in the Triassic carbonate rocks of the internal zone and points to a Tethysian influence in some periods, especially during the Late-Triassic transgressive stage. These data agree with the Germanic Triassic materials being deposited on an epicontinental platform flanked by the Iberian and the meso-Mediterranean plates and subjected to the influence of the Tethys domain, in agreement with the Alpine Triassic facies developed in the internal zone of the Betic Chain [55]. Therefore, a northern influx of sediments rich in zircons from the Iberian Massif, Pyrenees, Catalan Coastal Ranges, or Iberian Range would agree with this Tethyan bioprovince provenance and would discard the southern Morocco (Sephardic bioprovince) basin as the provenance area. In this regard, the Iberian Range evolution is widely marked by different rifting and post-rifting episodes that took place between the Early Permian and the Early Cretaceous ([54] and references therein). The first main rift episode was divided into three main different tectosedimentary phases based on the age of the sedimentary infilling, tectonic setting, and magmatic manifestations and bracketed into ranges of ~ 300 – 290 , ~ 285 – 275 , and ~ 260 Ma ([54] and references therein). These three main phases fit with the defined three zircon age populations of 292 ± 2 , 278 ± 3 , and 254 ± 3 Ma and agree with a plausible zircon source for the Ojén nappe's quartzites.

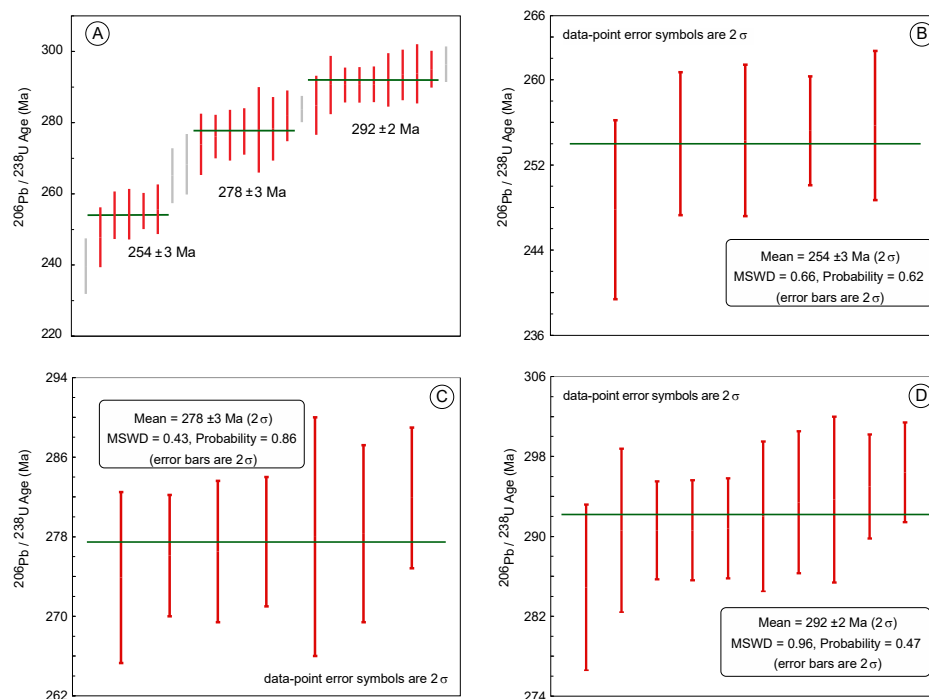


Figure 7. (A) Weighted mean ages of the Permian zircon populations of the integrated age distribution of both analyzed quartzites; (B–D) weighted mean ages of the integrated youngest zircon populations.

Finally, a well-defined Middle Ordovician detrital zircon population (460–465 Ma) was detected for the first time in the Betic Cordilleras. Investigations of the scarcity or presence of Ordovician zircon populations have been used in studies involving paleogeographic reconstruction that locate the Alborán microplate in either the southern passive margin of the Paleo-Thethys Ocean, as part of the European Cimmerian Superterrane [16], or in the south passive margin of the European Hunic superterrane [56,57], respectively. In this regard, the discovery of a Middle Ordovician population of detrital zircons would suggest that the Alborán microplate (meso-Mediterranean domain) was influenced by one of the peri-Mediterranean terranes that were detached from Gondwana to form the eastern branch of the Rheic Ocean [58]. In line with this interpretation, we propose that the European Hunic superterrane stands out as a likely source area for the supply of detrital zircons. A further consequence of such an interpretation is that the southern passive margin of the European Hunic superterrane constrains the palaeogeographic location of the Betic Cordilleras.

6. Conclusions

The U-Pb LA-ICP-MS age determinations of detrital zircons from two quartzite samples of the Ojén nappe, underlying the Ronda peridotites (Betic Cordilleras), suggest the following deductions:

1. The youngest detrital zircon population displays an age of 254 ± 3 Ma (Permian–Triassic) and a mean Th/U ratio of 0.34 that supports their Triassic sedimentation age and crystallization from a felsic magma, respectively.
2. Permian zircons are well-arranged in three main populations of 292 ± 2 Ma, 278 ± 3 Ma, and 254 ± 3 Ma, in agreement with the main age clusters reported for rhyolites and shallow crustal basaltic–andesite subalkaline rocks emplaced in transtensional Permian basins of the Variscan Orogen during the break-up of Pangea.
3. The quartzites of the Ojén nappe are characterized by the widespread presence of detrital zircon grains of Cisuralian (280–290 Ma), Ordovician (460–465 Ma), Ediacaran–Cryogenian (560–615 Ma) and Tonian–Stenian (950–975 Ma) ages and

by the scarcity of Mesoproterozoic ones. These zircon populations point to a sediment source from a Cadomian peri-Gondwanan terrane.

4. The well-defined Middle Ordovician detrital zircon population (460–465 Ma) strengthens the hypothesis that the Alborán microplate (meso-Mediterranean domain) could be located along the southern passive margin of the European Hunic superterrane.

Supplementary Materials: The following supporting information can be downloaded at: <https://www.mdpi.com/article/10.3390/min13040569/s1>, Figure S1: Permian zircon BSE images from studied quartzites. Table S1: LA-ICP-MS analytical results from studied quartzites.

Author Contributions: Conceptualization, J.J.E., J.C. and J.M.T.; methodology, J.J.E.; software, J.J.E.; validation, J.J.E., J.C. and J.M.T.; formal analysis, J.J.E.; investigation, J.J.E., J.C. and J.M.T.; data curation, J.J.E.; writing—original draft preparation, J.J.E.; writing—review and editing, J.M.T. and J.C.; visualization, J.J.E.; supervision, J.M.T.; project administration, J.C.; funding acquisition, J.C. All authors have read and agreed to the published version of the manuscript.

Funding: This research was funded by Ministerio de Economía, Industria y Competitividad/Agencia Estatal de Investigación/Fondo Europeo de Desarrollo Regional, European Union (grant number CGL2017-82976-P) and Grupos de Investigación, University of the Basque Country (grant number GIU20/017).

Data Availability Statement: The analytical data used in this study are available in the Supplementary Table S1 of the article or cited in peer-review references.

Conflicts of Interest: The authors declare no conflict of interest.

References

1. Dewey, J.F.; Helman, M.L.; Turco, E.; Hutton, D.W.H.; Knott, S.D. Kinematics of the western Mediterranean. In *Alpine Tectonics*; Coward, M.P., Dietrich, D., Park, R.G., Eds.; Geological Society of London, Special Publication: London, UK, 1989; Volume 45, pp. 265–283.
2. Navarro-Vilá, F.; Tubía, J.M. Essai d'une nouvelle différenciation des Nappes Alpujarrides dans le secteur occidental des Cordillères Bétiques (Andalousie, Espagne). *Comptes Rendus L'Académie Sci.* **1983**, *296*, 111–114.
3. Esteban, J.J.; Cuevas, J.; Tubía, J.M. Peri-Gondwanan provenance and geodynamic evolution of the Guadaiza nappe (Alpujarride Complex, Betic Cordilleras, Spain): Insights on the Paleotethyan paleogeography. *Minerals* **2021**, *12*, 325. [[CrossRef](#)]
4. Priem, H.N.A.; Boelrijk, N.A.; Hebeda, E.H.; Oen, I.S.; Verdurmen, E.A.T.; Verschure, R.H. Isotopic dating of the emplacement of the ultramafic masses in the Serrania de Ronda. *Contrib. Mineral. Petrol.* **1979**, *70*, 103–109. [[CrossRef](#)]
5. Monié, P.; Torres-Roldán, R.L.; García-Casco, A. Cooling and exhumation of the Western Betic Cordilleras, ⁴⁰Ar/³⁹Ar thermochronological constraints on a collapse terrane. *Tectonophysics* **1994**, *238*, 353–379. [[CrossRef](#)]
6. Sosson, M.; Morillon, A.C.; Bourgeois, J.; Féraud, G.; Poupeau, G.; Saint-Marc, P. Late exhumation stages of the Alpujarride Complex (western Betic Cordilleras, Spain): New thermochronological and structural data on Los Reales and Ojen nappe. *Tectonophysics* **1998**, *285*, 253–273. [[CrossRef](#)]
7. Sánchez-Rodríguez, L.; Gebauer, D. Mesozoic formation of pyroxenites and gabbros in the Ronda area (southern Spain), followed by Early Miocene subduction metamorphism and emplacement into the middle crust: U–Pb sensitive high-resolution ion microprobe dating of zircon. *Tectonophysics* **2000**, *316*, 19–44. [[CrossRef](#)]
8. Esteban, J.J.; Cuevas, J.; Tubía, J.M.; Sergeev, S.; Larionov, A. A revised Aquitanian age for the emplacement of the Ronda peridotites (Betic Cordilleras, southern Spain). *Geol. Mag.* **2011**, *148*, 183–187. [[CrossRef](#)]
9. Kozur, H.W.K.; Simon, O.J. Contribution to the Triassic microfauna and stratigraphy of the Betic Zone (southern Spain). *Rev. Esp. Micropaleontol.* **1972**, *30*, 143–158.
10. Kozur, H.W.K.; Mulder-Blanken, C.; Simon, O.J. On the Triassic of the Betic Cordilleras (southern Spain) with special emphasis on holothurian sclerites. In *Proceedings of the Koninklijke Nederlandse Akademie van Wetenschappen*; Series B; Palaeontology, geology, physics and chemistry; North-Holland: Amsterdam, The Netherlands, 1985; Volume 88, pp. 83–110.
11. Braga, J.C.; Martín, J.M. Distribución de las algas dasycladáceas en el Triás Alpujarride. *Cuad. Geol. Ibérica* **1987**, *11*, 475–489.
12. Durand-Delga, M.; Fontboté, J.M. Le problème de l'âge des nappes Alpujarrides d'Andalousie. *Rev. Géographie Phys. Géologie Dyn.* **1960**, *2*, 181–187.
13. Durand-Delga, M.; Fontboté, J.M. Le cadre structurale de la Méditerranée occidentale. In *Symposium on Geochemistry of Groundwater: 26th International Geological Congress, Paris, 1980*; Elsevier Scientific Pub. Co.: Amsterdam, The Netherlands, 1982; Volume 115, pp. 67–85.
14. Delgado, F.; Estévez, F.; Martín, J.M.; Martín-Algarra, A. Observaciones sobre la estratigrafía de la formación carbonatada de los mantos alpujarrides (Cordilleras Béticas). *Estud. Geol.* **1981**, *37*, 45–58.

15. Sánchez-Rodríguez, L. Pre-Alpine and Alpine Evolution of the Ronda Ultramafic Complex and Its Country-Rocks (Betic Chain, southern Spain): U–Pb SHRIMP Zircon and Fission Track Dating. Ph.D. Thesis, ETH Zurich, Zurich, Switzerland, 1998.
16. Esteban, J.J.; Tubía, J.M.; Cuevas, J.; Vegas, N.; Sergeev, S.; Larionov, A. Peri-Gondwanan provenance of pre-Triassic metamorphic sequences in the western Alpujarride nappes (Betic Cordillera, southern Spain). *Gondwana Res.* **2011**, *20*, 443–449. [[CrossRef](#)]
17. Tubía, J.M. Estructura de los Alpujarrides occidentales: Cinemática y condiciones de emplazamiento de las peridotitas de Ronda. *Bol. Geol. Min.* **1988**, *99*, 28–43.
18. Tubía, J.M.; Cuevas, J. High temperature emplacement of the Los Reales peridotite nappe (Betic Cordillera, Spain). *J. Struct. Geol.* **1986**, *8*, 473–482. [[CrossRef](#)]
19. Tubía, J.M.; Gil Iburguchi, J.I. Eclogites of the Ojén nappe: A record of subduction in the Alpujarride Complex (Betic Cordilleras, southern Spain). *J. Geol. Soc.* **1991**, *148*, 801–804. [[CrossRef](#)]
20. Esteban, J.J.; Cuevas, J.; Vegas, N.; Tubía, J.M. Deformation and kinematics in a melt bearing shear zone from the Western Betic Cordilleras (southern Spain). *J. Struct. Geol.* **2008**, *30*, 380–393. [[CrossRef](#)]
21. Vermeesch, P. How many grains are needed for a provenance study? *Earth Planet. Sci. Lett.* **2004**, *224*, 441–451. [[CrossRef](#)]
22. Paton, C.; Hellstrom, J.; Paul, B.; Woodhead, J.; Hergt, J. Iolite: Freeware for the visualization and processing of mass spectrometry data. *J. Anal. At. Spectrom.* **2011**, *26*, 2508. [[CrossRef](#)]
23. Paul, B.; Paton, C.; Norris, A.; Woodhead, J.; Hellstrom, J.; Hergt, J.; Greig, A. CellSpace: A module for creating spatially registered laser ablation images within the Iolite freeware environment. *J. Anal. At. Spectrom.* **2012**, *27*, 700–706. [[CrossRef](#)]
24. Petrus, J.A.; Kamber, B.S. VizualAge: A Novel Approach to Laser Ablation ICP-MS U–Pb Geochronology Data Reduction. *Geostand. Geoanal. Res.* **2012**, *36*, 247–270. [[CrossRef](#)]
25. Jackson, S.E.; Pearson, N.J.; Griffin, W.L.; Belousova, E.A. The application of laser ablation inductively coupled plasma mass spectrometry to in situ U–Pb zircon geochronology. *Chem. Geol.* **2004**, *211*, 47–69. [[CrossRef](#)]
26. Sláma, J.; Košler, J.; Condon, D.J.; Crowley, J.L.; Gerdes, A.; Hanchar, J.M.; Horstwood, M.S.; Morris, G.A.; Nasdala, L.; Norberg, N.; et al. Plešovice Zircon—A New Natural Reference Material for U–Pb and Hf Isotopic Microanalysis. *Chem. Geol.* **2008**, *249*, 1–35. [[CrossRef](#)]
27. Wiedenbeck, M.; Alle, P.; Corfu, F.; Griffin, W.L.; Meier, M.; Oberli, F.; von Quadt, A.; Roddick, J.C.; Spiegel, W. Three natural zircon standards for U–Th–Pb, Lu–Hf, trace element and REE analyses. *Geostand. Newsl.* **1995**, *19*, 1–23. [[CrossRef](#)]
28. Lana, C.; Farina, F.; Gerdes, A.; Alkmim, A.; Gonçalves, G.O.; Jardim, A.C. Characterization of zircon reference materials via high precision U–Pb LA-MC-ICP-MS. *J. Anal. At. Spectrom.* **2017**, *32*, 2011–2023. [[CrossRef](#)]
29. Ludwig, K.R. User’s manual for Isoplot 3.0 a Geochronological toolkit for Excel. *Berkeley Geochronol. Cent. Spec. Publ.* **2003**, *4*, 71.
30. Vermeesch, P. On the visualization of detrital age distributions. *Chem. Geol.* **2012**, *312–313*, 190–194. [[CrossRef](#)]
31. Zeck, H.P.; Whitehouse, M.J. Hercynian, Pan-African, Proterozoic and Archean ion-microprobe zircon ages for a Betic-Rif core complex, Alpine belt, W. Mediterranean- consequences for its P–T–t path. *Contrib. Mineral. Petrol.* **1999**, *134*, 134–149. [[CrossRef](#)]
32. Hoskin, P.W.; Schaltegger, U. The composition of zircon and igneous and metamorphic petrogenesis. *Rev. Mineral. Geochem.* **2003**, *53*, 27–62. [[CrossRef](#)]
33. Williams, I.S. Response of detrital zircon and monazite, and their U–Pb isotopic systems, to regional metamorphism and host-rock partial melting, Cooma Complex, southeastern Australia. *Aust. J. Earth Sci.* **2001**, *48*, 557–580. [[CrossRef](#)]
34. Rubatto, D. Zircon trace element geochemistry: Partitioning with garnet and the link between U–Pb ages and metamorphism. *Chem. Geol.* **2002**, *184*, 123–138. [[CrossRef](#)]
35. Stepanov, A.; Hermann, J.; Korsakov, A.V.; Rubatto, D. Geochemistry of ultrahigh-pressure anatexis: Fractionation of elements in the Kokchetav gneisses during melting at diamond-facies conditions. *Contrib. Mineral. Petrol.* **2014**, *167*, 1002. [[CrossRef](#)]
36. Rubatto, D. Zircon: The metamorphic mineral. *Rev. Mineral. Geochem.* **2017**, *83*, 261–295. [[CrossRef](#)]
37. Walzak, K.; Anczkiewicz, R.; Szczepanski, J.; Rubatto, D.; Kosler, J. Combined garnet and zircon geochronology of the ultra-high temperature metamorphism: Constraints on the rise of the Orlica-Snieznik Dome, NE Bohemian Massif, SW Poland. *Lithos* **2017**, *293*, 388–400. [[CrossRef](#)]
38. Wang, X.; Griffin, W.L.; Jie, C.; Pinyun, H.; Xiang, L.I. U and Th contents and Th/U ratios of zircon in felsic and mafic magmatic rocks: Improved zircon-melt distribution coefficients. *Acta Geol. Sin.-Engl. Ed.* **2011**, *85*, 164–174. [[CrossRef](#)]
39. López-Sánchez, M.A.; Aleinikoff, J.N.; Marcos, A.; Martínez, F.J.; Llana-Fúnez, S. An example of low-Th/U zircon overgrowths of magmatic origin in a late orogenic Variscan intrusion: The San Ciprián massif (NW Spain). *J. Geol. Soc.* **2015**, *173*, 282–291. [[CrossRef](#)]
40. Heaman, L.M.; Bowins, R.; Crocket, J. The chemical composition of igneous zircon suites: Implications for geochemical tracer studies. *Geochim. Cosmochim. Acta* **1990**, *54*, 1597–1607. [[CrossRef](#)]
41. Pereira, M.F.; Castro, A.; Chichorro, M.; Fernández, C.; Diaz-Alvarado, J.; Martí, J.; Rodríguez, C. Chronological link between deep-seated processes in magma chambers and eruptions: Permo-Carboniferous magmatism in the core of Pangaea (Southern Pyrenees). *Gondwana Res.* **2014**, *25*, 290–308. [[CrossRef](#)]
42. Kirkland, C.L.; Smithies, R.H.; Taylor, R.J.M.; Evans, N.; McDonald, B. Zircon Th/U ratios in magmatic environs. *Lithos* **2015**, *212*, 397–414. [[CrossRef](#)]
43. Puga, E.; Torres-Roldán, R.L. Geochemistry and age relationships of the metamorphosed mafic sills from Sierra de Enmedio and Sierra de Carrascoy (Eastern Betic Zone, Southeastern Spain). *Estud. Geol.* **1989**, *45*, 325–336. [[CrossRef](#)]

44. Morata, D.; Puga, E.; Demant, A.; Aguirre, L. Geochemistry and tectonic setting of the «ophites» from the external zones of the Betic Cordilleras (S. Spain). *Estud. Geol.* **1997**, *53*, 107–120. [[CrossRef](#)]
45. Puga, E. The Betic Ophiolitic Association (southeastern Spain). *Ophioliti* **1990**, *15*, 97–117.
46. Puga, E.; Díaz de Federico, A.; Fanning, M.; Nieto, J.M.; Rodríguez Martínez-Conde, J.Á.; Díaz Puga, M.Á.; Lozano, J.A.; Bianchini, G.; Natali, C.; Beccaluva, L. The Betic Ophiolites and the Mesozoic Evolution of the Western Tethys. *Geosciences* **2017**, *7*, 31. [[CrossRef](#)]
47. Nieto, J.M.; Puga, E.; Monié, P.; Díaz de Federico, A.; Jagoutz, E. High-pressure metamorphism and orthogneiss from the Mulhacén Complex (Betic Cordilleras, SE Spain). *Terra Nova Abstr. Supp.* **1997**, *1*, 22–23.
48. Aldaya, F.; García-Dueñas, V.; Navarro-Vilá, F. Los Mantos Alpujarrides del tercio central de las Cordilleras Béticas. Ensayo de correlación tectónica de los Alpujarrides. *Acta Geol. Hisp.* **1979**, *14*, 154–166.
49. Sánchez-Vizcaíno, V.L.; Gómez-Pugnaire, M.T.; Fernández-Soler, J.M. Petrological features of some Alpujarride, mafic igneous bodies from the Sierra de Almagro (Betic Cordilleras, Spain). *Rev. Soc. Geol. Esp.* **1991**, *4*, 321–335.
50. Martín-Rojas, I.; Somma, R.; Delgado, F.; Estévez, A.; Iannace, A.; Perrone, V.; Zamparelli, V. Triassic continental rifting of Pangaea: Direct evidence from the Alpujarride carbonates, Betic Cordillera, SE Spain. *J. Geol. Soc.* **2009**, *166*, 447–458. [[CrossRef](#)]
51. Torres-Roldán, R.; Poli, G.; Peccerillo, A. An early Miocene arc-tholeiitic magmatic dike event from the Alboran Sea—Evidence for precollisional subduction and backarc crustal extension in the westernmost Mediterranean. *Geol. Rundsch.* **1986**, *75*, 219–234. [[CrossRef](#)]
52. Turner, S.P.; Platt, J.P.; George, R.M.M.; Kelley, S.P.; Pearson, D.G.; Nowell, G.M. Magmatism associated with orogenic collapse of the Betic–Alboran Domain, SE Spain. *J. Petrol.* **1999**, *40*, 1011–1036. [[CrossRef](#)]
53. Esteban, J.J.; Tubía, J.M.; Cuevas, J.; Seward, D.; Larionov, A.; Sergeev, S.; Navarro-Vilá, F. Insights into extensional events in the Betic Cordilleras, southern Spain: New fission-track and U–Pb SHRIMP analyses. *Tectonophysics* **2013**, *603*, 179–188. [[CrossRef](#)]
54. López-Gómez, L.; Alonso-Azcárate, J.; Arche, A.; Arribas, J.; Fernández Barrenechea, J.; Borrueal-Abadía, V.; Bourquin, S.; Cadenas, P.; Cuevas, J.; De la Horra, R.; et al. Permian-Triassic Rifting Stage. In *The Geology of Iberia: A Geodynamic Approach. Regional Geology Reviews*; Quesada, C., Oliveira, J., Eds.; Springer: Berlin/Heidelberg, Germany, 2009; pp. 29–112.
55. Pérez-López, A.; Valera, F. Paleogeography, facies and nomenclature of the Triassic units in the different domains of the Betic Cordillera (S Spain). *Palaeogeogr. Palaeoclimatol. Palaeoecol.* **2007**, *254*, 606–626. [[CrossRef](#)]
56. Stampfli, G.M. Tethyan oceans. In *Tectonic and Magmatism in Turkey and the Surrounding Area*; Bozurt, E., Winchester, J.A., Piper, J.D.A., Eds.; Geological Society, London Special Publication: London, UK, 2000; pp. 1–23.
57. Von Raumer, J.F.; Stampfli, G.M. Gondwana derived microcontinents the constituents of the Variscan and Alpine collisional orogens. *Tectonophysics* **2003**, *365*, 7–22. [[CrossRef](#)]
58. Von Raumer, J.F.; Stampfli, G.M. The birth of the Rheic Ocean-Early Palaeozoic subsidence patterns and tectonic plate scenarios. *Tectonophysics* **2008**, *461*, 9–20. [[CrossRef](#)]

Disclaimer/Publisher’s Note: The statements, opinions and data contained in all publications are solely those of the individual author(s) and contributor(s) and not of MDPI and/or the editor(s). MDPI and/or the editor(s) disclaim responsibility for any injury to people or property resulting from any ideas, methods, instructions or products referred to in the content.